Journal of Materials Chemistry A

ROYAL SOCIETY OF CHEMISTRY

COMMUNICATION

View Article Online
View Journal | View Issue

Cite this: J. Mater. Chem. A, 2026, 14, 343

Received 10th September 2025
Accepted 2nd December 2025

DOI: 10.1039/d5ta07392h

rsc.li/materials-a

Effective and selective ethylene glycol electrooxidation with compositionally controlled Pt–Au bimetallic electrocatalysts

Hui Luo, *[a] Xianxian Xie,[b] Jiamin Sun,[c] Shaohui Guo [c] and Ivan Khalakhan *[b]

Controlling surface Pt and Au concentrations on PtAu nanoparticles *via* magnetron sputtering enables enhanced EGOR activity and glycolate selectivity. This improvement originates from structural modifications of Pt induced by adjacent Au atoms, which produces electronic and strain effects. These findings highlight surface composition engineering as a promising strategy for designing next-generation nanoparticle electrocatalysts with tailored performance.

Introduction

Polyethylene terephthalate (PET), made from repeating monomer units of terephthalic acid (TPA) and ethylene glycol (EG), is a widely used plastic product. In 2019, the consumption of PET reached 710 kton in the UK alone and accounted for 27% of all plastic types.[1] Although 44.2% of PET was recycled through mechanical recycling processes,[2] it cannot be recycled this way infinitely, as the material degrades over time and becomes unsuitable for producing food-grade containers. Therefore, end-of-life PET currently ends up in landfills or incineration facilities, while market demand for virgin PET still exceeds 600 kton per year.[3] In this regard, recent research has focused on chemical recycling, which can recover the pure monomer TPA from end-of-life PET for virgin PET manufacturing.[4–7] However, the by-product, ethylene glycol (EG) that contains contaminants from the waste stream, is miscible with water with a high boiling point. Therefore, it is hard to separate and has low economic value. It is crucial to also upcycle this by-product and generate additional benefits to promote the recycling rate. In this regard, the electrochemical ethylene glycol oxidation reaction (EGOR) to coproduce green H_2 and value-added chemicals at low potential constitutes a promising strategy. In this aspect, the market for the EG oxidation product glycolic acid has grown significantly, as it is a valuable commodity chemical but conventionally produced *via* petrochemistry, with applications in bio-polymer and cosmetic products and a market value reaching $531.5 million by 2027. Combining the production of green H_2 and glycolic acid, this approach would lead to an overall better economic and environmental impact. As a result, there is an increasing number of research studies on the EGOR in recent years.[8,9]

In general, a good EGOR catalyst should be able to activate the EG molecule at a relatively negative potential and have fast kinetics to reach high current density. At the same time, it should also exhibit high selectivity towards desired anodic chemical products, *e.g.* glycolic acid. Pt-based electrocatalysts are the state-of-the-art for EG electrooxidation. The Pt surface can adsorb EG molecules effectively and catalyse C–H, C–O, and C–C bond cleavage. However, because of the same reason, Pt also suffers from deactivation due to overoxidation and poisoning from formic acid and CO-like intermediates.[10,11]

[a]School of Engineering, Stag Hill Campus, University of Surrey, Guildford, GU2 7XH, UK. E-mail: hui_luo@surrey.ac.uk
[b]Department of Surface and Plasma Science, Faculty of Mathematics and Physics, Charles University, V Holešovičkách 2, 18000 Prague 8, Czech Republic
[c]College of Chemistry and Chemical Engineering, Taiyuan University of Technology, 030024, Taiyuan, Shanxi, China

Hui Luo

Dr Hui Luo (MRSC, MIMMM, FHEA) obtained her PhD in materials science from the Queen Mary University of London in 2019. She is currently a Royal Academy of Engineering research fellow in the School of Engineering and part of the Surrey Circular Economy Group at the University of Surrey, UK. She is a member of the RSC Energy Sector Interest Group Committee and has been shortlisted for the Journal of Materials Chemistry Lectureship in 2025. Her research focuses on developing efficient mechanocatalysis and electrocatalysis methods to convert biomass and plastic wastes into green hydrogen and high-value commodity chemicals.

Therefore, moving forward, it is important to modulate the Pt catalyst structure to achieve and balance high activity, high selectivity towards glycolic acid, and high poison tolerance.

In recent studies, attention has been paid to using Pt–Au bimetallic electrocatalysts for alcohol oxidation due to Au's high chemical stability and better poison tolerance. For example, Shao-Horn and co-workers found that surrounding surface Au atoms can effectively weaken CO binding on Pt in discrete Pt or Pt-rich clusters, thus enhancing activity towards CO and methanol oxidation.[12] Dai *et al.* prepared a series of AuPt nanoparticles for electrochemical glycerol-to-lactic acid conversion and showed that with an Au-enriched surface, the lactic acid selectivity can reach 73% at 0.45 V_{RHE}.[13] Although the authors did not investigate in detail the role of Au in tuning the product selectivity, such results clearly show the benefit of alloying Au in altering the reaction pathway. More recently, Li *et al.* designed a PtAu alloy catalyst on Ni foam (hp-PtAu/NF) for glycerol electrooxidation, which showed that the introduction of Au can significantly facilitate the adsorption of hydroxyl species, thus improving glycerol oxidation activity.[14]

However, so far there are limited studies on PtAu for the EGOR, especially those using structurally uniform and compositionally fine-tuned systems,[15,16] Herein, we present a systematic study of the EGOR on Pt–Au bimetallic electrocatalysts with different Pt to Au ratios. By tuning the surface composition of Pt–Au, we aim to establish the correlation between surface composition and catalytic performance for the EGOR ($C_2H_6O_2 + H_2O \rightarrow C_2H_4O_3 + 2H_2$), and provide preliminary insights into the influence of electronic structure changes within the PtAu electrodes.

Results and discussion

A series of Pt–Au bimetallic alloys with the same thickness of 10 nm but different compositions were prepared using a magnetron co-sputtering technique (Fig. 1a), referred to as $PtAu_5$, $PtAu_{10}$ and $PtAu_{20}$, corresponding to $Pt_{95}Au_5$, $Pt_{90}Au_{10}$ and $Pt_{80}Au_{20}$, respectively. These samples are prepared using parameters identical to those in our previous work.[17] In addition, pure Pt and Au electrodes were also fabricated using the single targets as control samples.

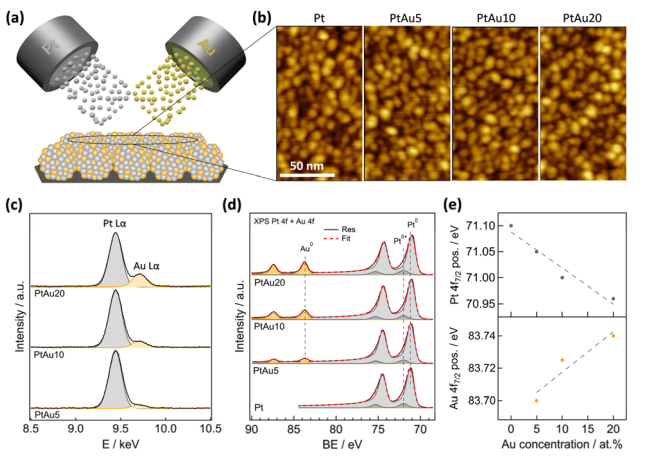

Fig. 1 (a) Illustration of the magnetron sputtering deposition process, (b) AFM images of the as-deposited pure Pt and Pt–Au alloy catalysts, (c) EDX and (b) XPS spectra acquired for the as-deposited Pt–Au alloy catalysts and pure Pt, and (e) Pt $4f_{7/2}$ and Au $4f_{7/2}$ peak positions extracted from the XPS spectra shown in (d).

The morphology of the as-deposited layers was examined by atomic force microscopy (AFM). As shown in Fig. 1b, all catalysts exhibit homogeneously distributed grains, characteristic of sputter-deposited thin films,[18] with nearly identical morphologies, indicating that morphology will not impact further catalytic activity measurements. The composition of the samples was characterized using bulk-sensitive energy-dispersive X-ray spectroscopy (EDX) and surface-sensitive X-ray photoelectron spectroscopy (XPS) techniques. Fig. 1c displays the Pt Lα and Au Lα EDX spectra, while Fig. 1d shows the Pt 4f and Au 4f XPS spectra, used for quantitative analysis. The corresponding survey spectra are provided in Fig. S1. The EDX spectra of the as-deposited Pt–Au alloys were deconvoluted into two peaks at 9.44 and 9.71 keV, assigned to Pt Lα and Au Lα, respectively. The XPS core levels exhibit three doublets at about 84.0/87.7, 71.1/74.4, and 72.0/75.3 eV, attributed to Au^0, Pt^0 and $Pt^{\delta+}$ states, respectively.[17,19,20] The presence of a small fraction of $Pt^{\delta+}$ states could be related to adsorbate-induced partial surface oxidation of platinum during sample transfer through air.[20] A closer look at the XPS spectra reveals a continuous shift of the Pt 4f and Au 4f regions (highlighted in Fig. 1d as Pt $4f_{7/2}$ and Au $4f_{7/2}$ positions) with increasing Au concentration in the alloy, indicating changes in the electronic structures of both Pt and Au due to alloying. More comprehensive characterization of identically prepared Pt–Au samples, including CO stripping, synchrotron radiation photoelectron spectroscopy and X-ray diffraction, can be found in our previous work, which demonstrates that the precise adjustment of the amount of gold in the Pt–Au alloy allows accurate tuning of platinum geometrical and electronic structures.[17] Quantitative analysis of the EDX and XPS spectra reveals nearly identical Pt–Au catalyst compositions (see Table S1), confirming that the Au content on the surface matches that in the bulk. This indicates a homogeneous Pt–Au atomic ratio across the deposited layers, consistent with our earlier study.

Given that the thin film electrodes possess a homogenous PtAu ratio, flat surface and fine-tuned composition, they are ideal for conducting fundamental studies of the EGOR, as factors such as surface roughness-induced mass transport differences and composition inhomogeneity across different catalysts are largely limited. However, we have to point out that electrodes with such a thin film configuration tend to be unstable due to delamination between the thin film and substrate and therefore cannot be used in longer term stability measurements. Herein, the electrochemical activity of all the film electrodes was first evaluated in 1 M NaOH with and without 0.1 M EG addition in three-electrode configurations. Comparing the cyclic voltammetry (CV) (Fig. 2a) and linear sweep voltammetry (LSV) (Fig. 2b) profiles in the presence of EG, it can be seen that increasing the surface Au concentration enhanced the intrinsic activity of the EGOR compared with pure Pt, with the starting potential negatively shifted to lower

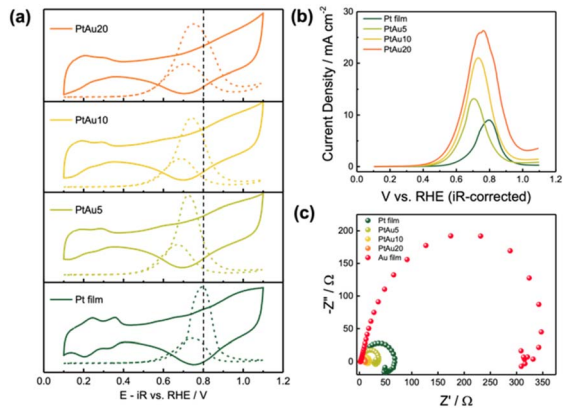

Fig. 2 Electrochemical EGOR activity of the PtAu and Pt electrodes. (a) CV profiles in 1 M NaOH with/without 0.1 M EG; scan rate: 50 mV s^{-1}. (b) LSV profiles in 0.1 M EG + 1 M NaOH; scan rate: 10 mV s^{-1}. (c) EIS Nyquist plot in 0.1 M EG + 1 M NaOH at 0.7 V_{RHE}; frequency: 100 kHz to 0.1 Hz.

potentials. The current density at the peak potentials also follows the trend $PtAu_{20}$ > $PtAu_{10}$ > $PtAu_5$ > Pt. We hypothesize the enhancement in the EGOR kinetics of PtAu catalysts to stem from the modified electronic structure of surface Pt that is surrounded by Au neighbors, which results in a weakened binding strength of carbon-based intermediate species. This hypothesis is supported by previous studies on single crystals with a similar Pt rich surface configuration, which have shown a weaker CO binding contribution from the next nearest Au atoms.[21,22] However, since the alloying with Au has also induced tensile strain in the electrode originating from the larger Au atom, as evidenced by the XRD results in our previous work,[17] we cannot rule out the role of the strain effect in controlling the PtAu electrodes' EGOR activity. In bimetallic systems, these electronic and geometric effects always occur simultaneously, influencing the catalytic properties together. As a result, it is challenging to isolate the contribution of each effect experimentally or theoretically, and the observed changes in activity or stability are typically a combination of both factors.[23]

We then extended the potential range to observe distinctive features related to surface activity on Au sites. As shown in Fig. S2, after alloying with Au, redox peaks associated with Au oxidation and reduction can be observed at near 1.2 V_{RHE} and 1 V_{RHE}, respectively, indicating the presence of Au at the electrochemical interface. Such peaks became more pronounced with higher Au loading, further validating the material characterization results. It can be noticed that a tiny EG oxidation peak attributed to EG oxidation on Au (Fig. S3) can be observed near 1.1 V_{RHE} and its potential remains unchanged. Such results suggest that the reactivity of Au sites in the PtAu electrodes remains constant, and the increased EGOR activity is attributed mainly to the Pt sites that are affected by the nearby Au atoms,[24] in line with the hypothesis above. To gain more understanding of how surface Au enhances the EGOR performance of Pt sites, we then performed electrochemical EIS measurements in the presence of EG. As shown in Fig. 2c, among all the electrodes, $PtAu_{20}$ exhibits the smallest semicircle, suggesting the lowest charge transfer resistance at the electrochemical interface. Such an improved interfacial charge transfer process enables fast, concerted proton-coupled electron transfer during the EGOR, improves the reaction kinetics and thus lowers the overpotential, as seen in Fig. 2b. Next, we took a closer look at the CVs of all Pt-based electrodes in the 1 M NaOH supporting electrolyte shown in Figure S4. In the potential region of 0.4–0.7 V_{RHE}, where *OH adsorption takes place on Pt sites, $PtAu_5$ and $PtAu_{10}$ exhibited a peak at ~0.6 V_{RHE}, with slightly higher current density and a shift towards more negative potentials. In contrast, the $PtAu_{20}$ electrode showed a decreased current density in this region compared to the Pt electrode. It is well known that surface adsorbed *OH is a key reactant for EG oxidation.[25] Therefore, although higher Au loading has led to lower charge transfer resistance, an excess amount of Au may hinder the *OH adsorption on Pt sites, as Au, unlike Ru or Sn, is much more inert.[12] These competing factors determine that there is an optimal Pt–Au composition for the EGOR.

Subsequently, we investigated the product selectivity as a function of applied potential by performing chronoamperometry measurements. The instantaneous oxidation products at different potentials were analysed by high-performance liquid chromatography (HPLC) using the calibration curve shown in Fig. S6. Given the low concentration of the generated products, we have calibrated the instrument to a range within 0.01–2.5 mM. As shown in Fig. 3a–c and S7, on all electrodes, only glycolate (salt form of glycolic acid), oxalate (salt form of oxalic acid) and formate (salt form of formic acid) were detected as the stable products in liquid electrolyte, which can represent the product distribution in the EGOR system. It should be noted that carbonate may also be formed as an over-

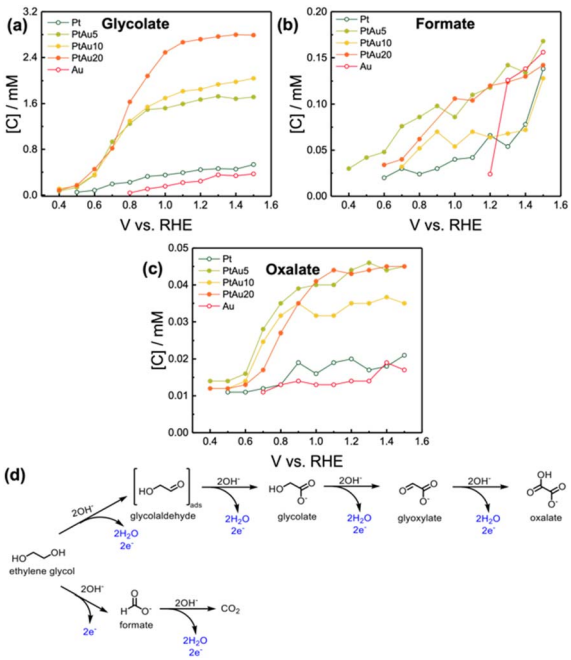

Fig. 3 EGOR product concentration as a function of potential on different electrodes analysed by HPLC: (a) glycolate, (b) formate, and (c) oxalate. The corresponding chronoamperometry profiles are included in Fig. S5. (d) Proposed reaction pathway.

oxidation product of EG, but its presence cannot be detected by HPLC. The first observed product, glycolate, was detected from 0.4 V_{RHE} among all electrodes containing Pt ($PtAu_5$, $PtAu_{10}$, $PtAu_{20}$, and Pt), while on the Au electrode it did not appear until 0.8 V_{RHE}, in good agreement with the observed starting potential seen in CV and LSV measurements as well as previous studies.[10,26] Specifically, the glycolate concentration in PtAu electrodes is much higher than that of Pt and Au electrodes. In contrast, the minor product formate concentration appeared to be in a similar range among all film electrodes, suggesting that the enhanced electrochemical activity originated from the conversion of EG to glycolate. According to Li *et al.*, such a change in product selectivity could be attributed to the optimized adsorption geometry of alcohol molecules on the catalyst surface. Rather than binding through two C atoms, the Pt–Au surface favors the binding configuration of one terminal C atom, which effectively prevents C–C bond breaking into formate.[14] Furthermore, alloying with Au may also facilitate glycolate desorption from the catalyst surface, preventing over-oxidation to oxalate and formate.

Different from the Pt-based electrodes, on Au films, the formate product was not detected until 1.2 V_{RHE}, 400 mV more positive than the formation of glycolate. The formate concentration also increased rapidly at higher potential compared to that of the Pt-based electrodes. Such a potential (>1.2 V_{RHE}) is related to surface Au oxidation as seen in Fig. S2 and previous reports,[25] which may suggest that as the Au oxidation state changes, the EG oxidation pathway shifts towards promoting C–C cleavage.

Electrochemical *in situ* Raman spectroscopy was employed to further intuitively clarify dynamic changes in the $PtAu_{20}$ electrode during the EGOR process in 1 M NaOH with 0.1 M EG addition at various potentials. Fig. S8 shows strong peaks at around 490 cm^{-1}, corresponding to Pt–C stretching mode.[27] The peaks at 603 cm^{-1} and 798 cm^{-1} are assigned to the bending mode of δ (Pt–O)[28] and δ (Au–O),[29,30] respectively. The bands around 1055 cm^{-1} and 1083 cm^{-1}, which can be assigned to the intermediate bonded with the carbon atoms of EG,[30] remain unchanged over the studied potential range. This phenomenon can be due to different reasons. First, EG adsorption on the $PtAu_{20}$ surface may be excessive, in which the signals from the reacted molecules cannot be distinguished. Secondly, as EG is a strong adsorbing molecule like glycerol on the Pt surface, certain reacted species may not desorb, especially at higher potentials where the adsorption energy is higher. Finally, despite the presence of Au enabling a surface enhanced Raman effect, the signals may still be disturbed by the bulk electrolyte, and therefore the subtle features from the surface interface are overshadowed. Therefore, no qualitative results are derived from the *in situ* Raman study, and further studies, such as roughing the surface for stronger surface enhancement, are required for future work.

Conclusions

In summary, we show that controlling the surface atomic concentration of Au on PtAu nanoparticles is critical for enhancing the EGOR activity. By fine-tuning the surface Au composition using magnetron sputtering, both the catalytic activity and selectivity towards glycolate can be enhanced. We hypothesise that such enhancement in the EGOR kinetics of PtAu catalysts stems from the modified electronic structure of surface Pt that is surrounded by Au neighbors, and future work will focus on mechanistic investigations to correlate surface composition, electronic structure and electrochemical performance. Our work demonstrates that electronic structure control through surface composition manipulation represents another avenue for designing a future generation of nanoparticle electrocatalysts.

Conflicts of interest

There are no conflicts to declare.

Data availability

The data supporting this article have been included as part of the supporting information (SI). Supplementary information: experimental section, material characterisation, and additional electrochemical results. See DOI: https://doi.org/10.1039/d5ta07392h.

Raw data for this article, including electrochemical testing and liquid product from HPLC, are available at figshare: https://doi.org/10.6084/m9.figshare.30090457.v2.

Acknowledgements

HL acknowledges support from the Royal Society Research Grant (RG\R1\241164) and the Royal Academy of Engineering Research Fellowship (RF-2324-23-176). This study was completed with the assistance of infrastructure funded by the Ministry of Education, Youth and Sports (MEYS), Czech Republic, through project LM2023072.

References

1 H. Zhou, Y. Ren, Z. Li, M. Xu, Y. Wang, R. Ge, X. Kong, L. Zheng and H. Duan, *Nat. Commun.*, 2021, **12**, 4679.
2 Environment, Food and Rural Affairs Committee, The price of plastic: ending the toll of plastic waste, *Third Report of Session 2022-23*, 2022.
3 Plastic Recycling, https://www.bpf.co.uk/sustainability/plastics_recycling.aspx, accessed 18 July 2025.
4 A. Singh, N. A. Rorrer, S. R. Nicholson, A. C. Carpenter, J. E. Mcgeehan and G. T. Beckham, *Joule*, 2021, **5**, 2479–2503.
5 Y. Peng, J. Yang, C. Deng, J. Deng, L. Shen and Y. Fu, *Nat. Commun.*, 2023, **14**, 3249.
6 S. Ügdüler, K. M. Van Geem, R. Denolf, M. Roosen, N. Mys, K. Ragaert and S. De Meester, *Green Chem.*, 2020, **22**, 5376–5394.
7 N. P. Murphy, S. H. Dempsey, J. S. DesVeaux, T. Uekert, A. C. Chang, S. Mailaram, M. Alherech, H. M. Alt, K. J. Ramirez, B. Norton-Baker, E. L. Bell, C. A. Singer,

A. R. Pickford, J. E. McGeehan, M. J. Sobkowicz and G. T. Beckham, *Nat. Chem. Eng.*, 2025, **2**(5), 309–320.
8 H. Luo, J. Barrio, N. Sunny, A. Li, L. Steier, N. Shah, I. E. L. Stephens and M. M. Titirici, *Adv. Energy Mater.*, 2021, 2101180.
9 J. J. Zhao, H. R. Zhu, C. J. Huang, M. H. Yin and G. R. Li, *J. Mater. Chem. A*, 2025, **13**, 3236–3272.
10 L. Xin, Z. Zhang, J. Qi, D. Chadderdon and W. Li, *Appl. Catal., B*, 2012, **125**, 85–94.
11 Y. Kwon, K. J. P. Schouten and M. T. M. Koper, *ChemCatChem*, 2011, **3**, 1176–1185.
12 J. Suntivich, Z. Xu, C. E. Carlton, J. Kim, B. Han, S. W. Lee, N. Bonnet, N. Marzari, L. F. Allard, H. A. Gasteiger, K. Hamad-Schifferli and Y. Shao-Horn, *J. Am. Chem. Soc.*, 2013, **135**, 7985–7991.
13 C. Dai, L. Sun, H. Liao, B. Khezri, R. D. Webster, A. C. Fisher and Z. J. Xu, *J. Catal.*, 2017, **356**, 14–21.
14 Y. Li, X. Wei, R. Pan, Y. Wang, J. Luo, L. Li, L. Chen and J. Shi, *Energy Environ. Sci.*, 2024, **17**, 4205–4215.
15 C. Jin, Y. Song and Z. Chen, *Electrochim. Acta*, 2009, **54**, 4136–4140.
16 Y. Kim, H. J. Kim, Y. S. Kim, S. M. Choi, M. H. Seo and W. B. Kim, *J. Phys. Chem. C*, 2012, **116**, 18093–18100.
17 X. Xie, V. Briega-Martos, R. Farris, M. Dopita, M. Vorokhta, T. Skála, I. Matolínová, K. M. Neyman, S. Cherevko and I. Khalakhan, *ACS Appl. Mater. Interfaces*, 2023, **15**, 1192–1200.
18 A. L. M. Sandhya, P. Pleskunov, M. Bogar, X. Xie, P. A. Wieser, M. Orság, T. N. Dinhová, M. Dopita, R. Taccani, H. Amenitsch, A. Choukourov, I. Matolínová and I. Khalakhan, *Surf. Interfaces*, 2023, **40**, 103079.
19 X. Xie, V. Briega-Martos, P. Alemany, A. L. Mohandas Sandhya, T. Skála, M. G. Rodríguez, J. Nováková, M. Dopita, M. Vorochta, A. Bruix, S. Cherevko, K. M. Neyman, I. Matolínová and I. Khalakhan, *ACS Catal.*, 2025, **15**, 234–245.
20 R. Mom, L. Frevel, J. J. Velasco-Vélez, M. Plodinec, A. Knop-Gericke and R. Schlögl, *J. Am. Chem. Soc.*, 2019, **141**, 6537–6544.
21 M. O. Pedersen, S. Helveg, A. Ruban, I. Stensgaard, E. Lægsgaard, J. K. Nørskov and F. Besenbacher, *Surf. Sci.*, 1999, **426**, 395–409.
22 M. Eyrich, T. Diemant, H. Hartmann, J. Bansmann and R. J. Behm, *J. Phys. Chem. C*, 2012, **116**, 11154–11165.
23 C. Lim, A. R. Fairhurst, B. J. Ransom, D. Haering and V. R. Stamenkovic, *ACS Catal.*, 2023, **13**, 14874–14893.
24 P. N. Duchesne, Z. Y. Li, C. P. Deming, V. Fung, X. Zhao, J. Yuan, T. Regier, A. Aldalbahi, Z. Almarhoon, S. Chen, D. Jiang, N. Zheng and P. Zhang, *Nat. Mater.*, 2018, **17**(11), 1033–1039.
25 L. Pérez-Martínez, L. Balke and A. Cuesta, *J. Catal.*, 2021, **394**, 1–7.
26 Y. Kwon, S. J. Raaijman and M. T. M. Koper, *ChemCatChem*, 2014, **6**, 79–81.
27 S. C. S. Lai, S. E. F. Kleyn, V. Rosca and M. T. M. Koper, *J. Phys. Chem. C*, 2008, **112**, 19080–19087.
28 Y. F. Huang, P. J. Kooyman and M. T. M. Koper, *Nat. Commun.*, 2016, **7**, 12440.
29 A. Das, B. Mohapatra, V. Kamboj and C. Ranjan, *ChemCatChem*, 2021, **13**, 2053–2063.
30 Y. Li, X. Wei, R. Pan, Y. Wang, J. Luo, L. Li, L. Chen and J. Shi, *Energy Environ. Sci.*, 2024, **17**, 4205–4215.